metals

Article

Optimization of Strength and Plasticity in Layered Aluminum Composites Through High-Pressure Torsion Treatment

Alexey Evstifeev [1], Aydar Mavlyutov [1,2,*], Artem Voropaev [3] and Darya Volosevich [3]

[1] Mathematics and Mechanics Faculty, Saint Petersburg State University, Saint Petersburg 199034, Russia; a.evstifeev@spbu.ru
[2] Ioffe Institute, Saint Petersburg 194021, Russia
[3] World-Class Research Center, State Marine Technical University, Saint Petersburg 119991, Russia; a.voropaev@ilwt.smtu.ru (A.V.); d.volosevich@ilwt.smtu.ru (D.V.)
* Correspondence: a.mavlyutov@spbu.ru

Abstract: The development of high-strength aluminum alloys with improved ductility is a crucial challenge for modern materials science, as high strength and ductility tend to be mutually exclusive properties. In this work, the composite material was fabricated using wire arc additives manufactured from AA1050 (commercially pure aluminum) and AA5056 (an Al–Mg system alloy) aluminum alloys. It was demonstrated that the addition of a lower-strength material into a high-strength matrix enhances the potential for deformation localization and results in an increased plasticity of the composite material. A further strengthening of the composite material was achieved through its deformation by a high-pressure torsion (HPT) technique. The mechanical properties of the material were thoroughly investigated before and after the HPT treatment. Static strength and plasticity were analyzed as a function of the deformation degree. Microstructural analysis was performed using scanning electron microscopy and X-ray diffraction. The optimal deformation route, providing the best combination of mechanical properties, was experimentally identified, along with key microstructural parameters of the formed composite with a bimodal grain structure. A deformation level corresponding to 36% of shear stress provides a yield stress of up to 570 MPa, an ultimate tensile strength of up to 664 MPa, and a relative elongation to failure of up to 7%. As a result of the deformation treatment, characteristic substructures with dimensions of ~250 nm and >1000 nm are formed, with a volume ratio of approximately 80/20.

Keywords: wire arc additive manufacturing; high-pressure torsion; composite materials; aluminum–magnesium alloys; bimodal structure

Citation: Evstifeev, A.; Mavlyutov, A.; Voropaev, A.; Volosevich, D. Optimization of Strength and Plasticity in Layered Aluminum Composites Through High-Pressure Torsion Treatment. *Metals* **2024**, *14*, 1445. https://doi.org/10.3390/met14121445

Academic Editor: Antonio Riveiro

Received: 4 November 2024
Revised: 12 December 2024
Accepted: 14 December 2024
Published: 17 December 2024

1. Introduction

Aluminum–magnesium (Al–Mg) alloys have garnered considerable interest owing to their versatile applications and highly desirable properties. These alloys are widely utilized across a range of industries, including the aerospace, maritime, and automotive sectors, primarily because of their unique combination of low density, impressive mechanical strength, and exceptional resistance to corrosion [1,2]. Their lightweight nature not only enhances fuel efficiency in transportation applications but also makes them ideal for structures where weight reduction is critical without compromising durability or performance. The primary concern lies in the fact that as the strength of aluminum alloys increases, their ductility tends to decrease significantly, which can pose challenges in applications requiring a balance of both high strength and adequate formability. The development of aluminum alloys that successfully combine improved mechanical strength with enhanced functional plasticity represents a considerable challenge in the field of modern materials science.

One promising approach for developing aluminum alloys with improved strength and functional plasticity is the creation of composite materials that combine the beneficial properties of different individual components. Wire arc additive manufacturing (WAAM) is an

advanced process that utilizes directed energy to deposit materials layer by layer, enabling the creation of complex structures with high precision [3–6]. This innovative technology holds significant potential for producing composite materials by integrating different components, each contributing unique properties to the final product [7–12]. Wire arc additive manufacturing (WAAM) has been successfully employed to produce laminated metal composite materials, which consist of alternating layers of ductile and high-strength materials. These composites are often made using metals such as aluminum, nickel, steel, and titanium alloys, each selected for its specific mechanical and functional properties [13–15]. The exceptional properties of Al–Mg alloys manufactured using WAAM have been verified by numerous scientific teams on a variety of alloys, including 5056 [16–18], 5087 [19], and 5356 [20]. By strategically layering these materials, WAAM enables the creation of structures that combine the toughness and formability of ductile layers with the strength and durability of high-strength layers. This layered approach enhances the overall performance of the composite. Composite materials with a layered structure exhibit high ductility in areas where maximum stresses occur, allowing for a more uniform distribution of loads and deformations within the structure. This prevents failure and leads to the widespread use of these materials in industries such as aerospace, shipbuilding, and automotive manufacturing to produce lightweight, high-performance parts.

Severe plastic deformation (SPD) techniques have shown promising results in improving the mechanical properties of conventional Al–Mg alloys and those produced by the WAAM process [18,21–24]. For example, Al–Mg alloys with a magnesium content ranging from 0.5 to 2 wt.%, processed through equal-channel angular pressing (ECAP), demonstrate a significant grain refinement and an increase in dislocation density [25]. When subjected to high-pressure torsion (HPT), ultrafine-grained (UFG) Al–Mg alloys maintain acceptable levels of ductility as long as the Mg content does not exceed 2.5 wt.% [26]. However, increasing the Mg concentration to 4.1 wt.% leads to a noticeable reduction in the ductility of HPT-treated alloys [27]. At even higher Mg levels, reaching 4.5 wt.%, plastic deformation in materials processed by HPT becomes entirely inhibited [26–30]. This issue can be addressed by incorporating a lower-strength, ductile material into a high-strength matrix during WAAM fabrication. A composite consisting of commercially pure aluminum, which exhibits excellent ductility in a coarse-grain state, and a strain-hardening Al–Mg alloy has the potential to create materials that overcome the trade-off between strength and ductility. Further HPT treatments can be used to achieve optimal strength and deformation properties.

In this study, we investigated the microstructural features and deformation behaviors of aluminum composite laminates manufactured using the WAAM process with AA1050 and AA5056 alloys. The AA5056 alloy served as the base material, while layers of the more ductile AA1050 alloy were added to enhance the localized plastic deformation.

2. Materials and Methods

The composite materials for investigation were created using a WAAM setup from two commercial aluminum alloys—AA5056 (4.98 Mg, 0.14 Mn, and 0.09 Fe (wt.%) in Al balance) and AA1050 (0.2 Si and 0.12 Fe (wt.%) in Al balance). The initial materials were provided by the Avial Experimental Plant (Moscow, Russia) in the form of wires with a diameter of 1.2 mm. The composite material was fabricated using a direct arc deposition system, employing Fronius equipment (Figure 1a) with cold metal transfer (CMT) technology. A TPS 500i arc source (Fronius international GmbH, Guttenbach, Austria) was used, and the motion system was controlled by a Fanuc M-710iC industrial robot (Fanuc Co., Ltd., Osino-Mura, Yamanashi Prefecture, Japan). The technology employed in this study is based on metal inert gas (MIG) welding utilizing a continuous solid wire electrode. CMT was applied to minimize the heat input during the deposition process. High-purity argon was used as a shielding gas to protect the weld pool from atmospheric contamination. The manufacturing process began with two initial welding passes at 120 A, 10 mm/s, and 14.8 V, which served to preheat the substrate and ensure the proper adhesion of the

subsequent layers. The deposition was carried out at the same current and voltage with a travel speed of 10–15 mm/s; the offset between adjacent beads was 3.2 mm, and the wire feed was 8.1 m/min. The composite samples were obtained by depositing alternating layers of the AA5056 and AA1050 aluminum alloys stacked on top of each other to reach the following final dimensions of the ingot: 60 mm in height, 30 mm in width, and 100 mm in length. During the production of the ingot, spools of different alloys were used alternately. Figure 1b provides a visual overview of the printing process, illustrating the key system components. The composite ingot obtained by WAAM is shown in Figure 1c. The ingots were homogenized at 480 °C for 2 h to eliminate the influence of secondary phases formed during welding.

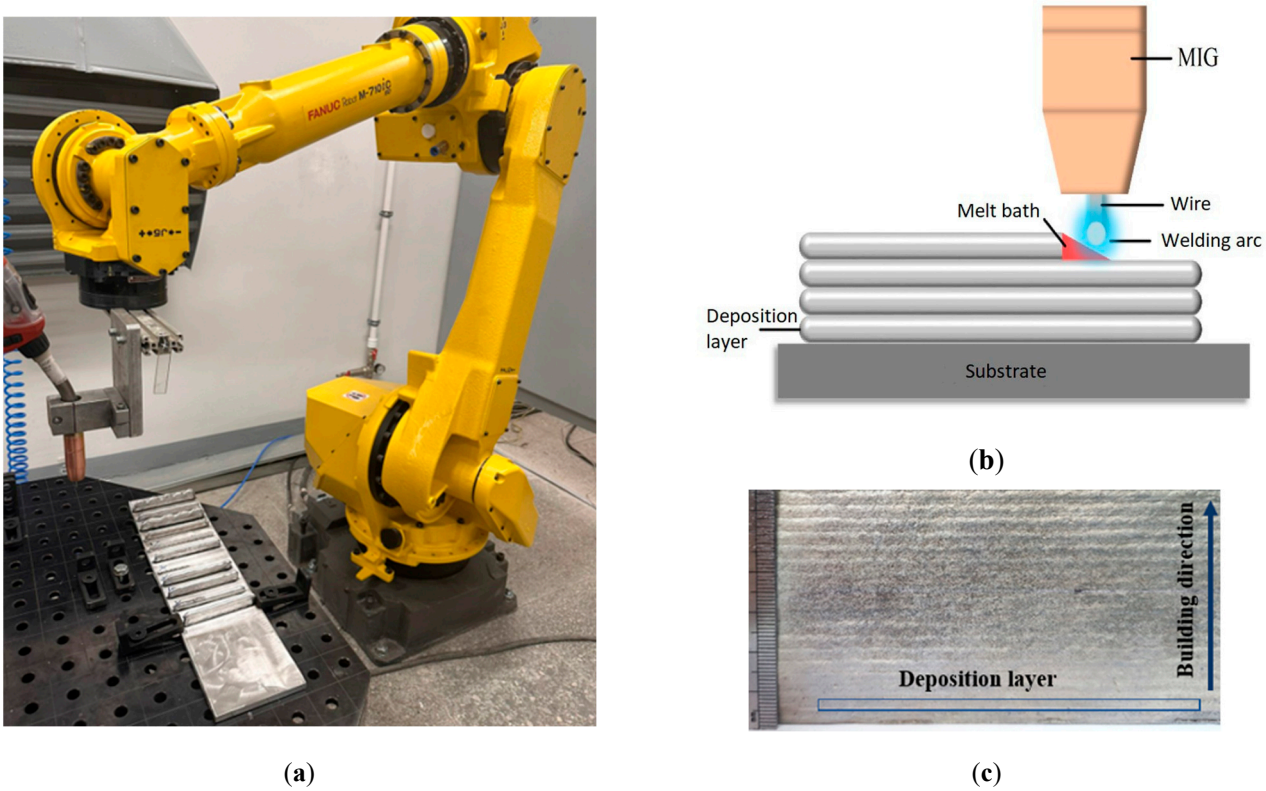

(**a**) (**b**) (**c**)

Figure 1. WAAM installation based on Fronius and Fanuc equipment (**a**); schematic representation of the WAAM technology process (**b**); and WAAM sample as a combination of AA5056 and AA1050 aluminum alloys (**c**).

Uniaxial tensile tests were performed using a Shimadzu AG-50kNX testing machine (Kyoto, Japan) at a constant strain rate of 10^{-3} s^{-1} on flat specimens with a width and thickness of the working parts of 4 and 1.5 mm, respectively. At least three samples were tested for each state. The length of the working part varied depending on the number of AA1050 layers and their orientation relative to the working part of the specimen. Figure 2a shows the schematic arrangement of the specimens in the composite volume with a single 2.5 mm thick AA1050 layer oriented perpendicular to the working part (further denoted as the 1L_90 sample) and at a 45° angle to the working part (further denoted as the 1L_45 sample). The length of the working part of the 1L_90 and 1L_45 samples was 15 mm. Figure 2b illustrates the schematic arrangement of the specimens in the composite volume with alternating layers of 2.5 mm thick AA1050 and 5 mm thick AA5056. The length of the working part of the specimens with two AA1050 layers oriented at 90° to the working part was 15 mm (the 2L_90 sample in Figure 2b). The length of the working part in samples with two AA1050 layers oriented at 45° to the working part was 20 mm (the 2L_45 sample in Figure 2b). For samples with three AA1050 layers oriented at 90° to the working part, the length of the working part was 25 mm (the 3L_90 sample in Figure 2b).

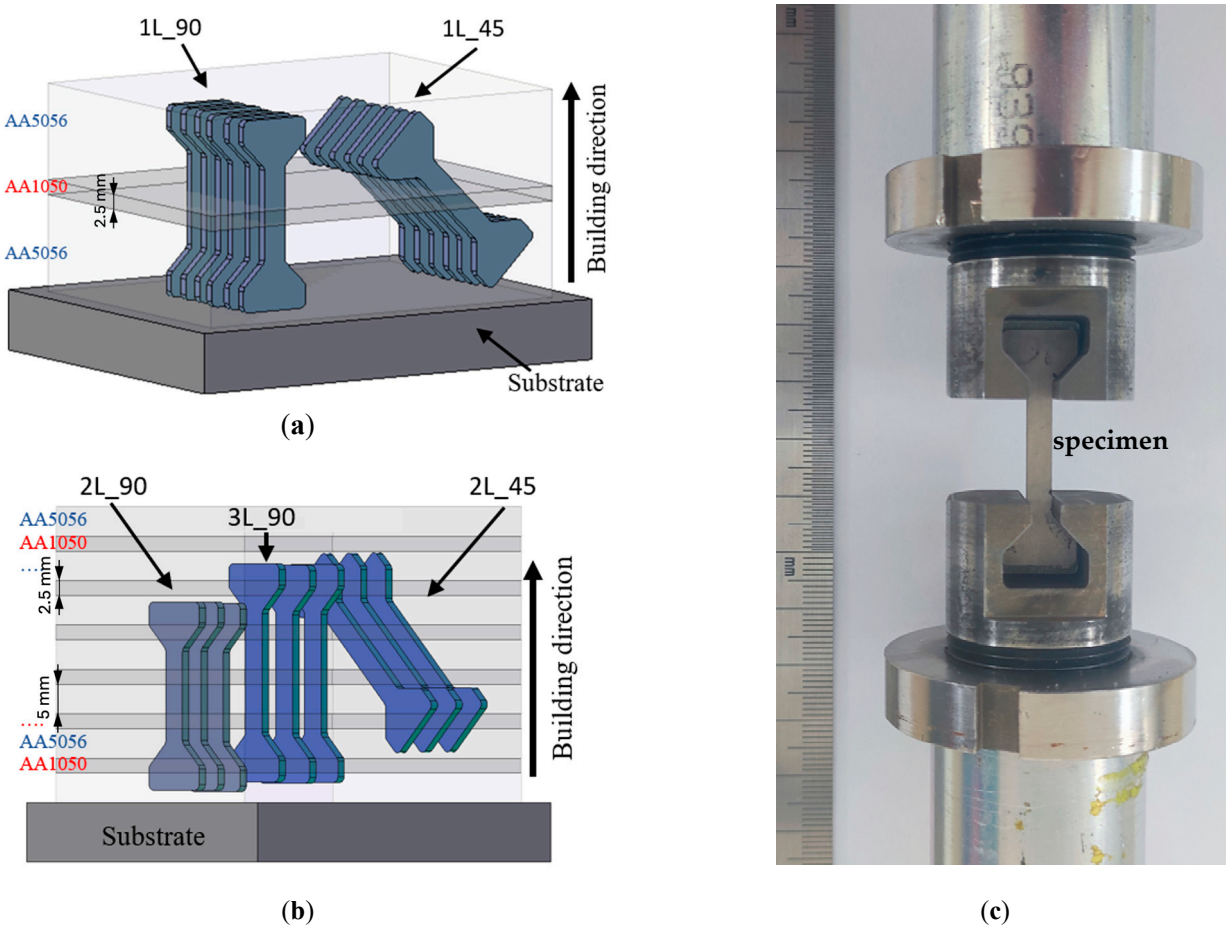

Figure 2. The arrangement of specimens within the composite volume: (**a**) single 2.5 mm thick layer of AA1050; (**b**) alternating 2.5 mm thick layers of AA1050 and 5 mm thick layers of AA5056; and (**c**) the clamping of the specimen within the grips.

For the high-pressure torsion treatment, samples in the form of disks with a diameter of 20 mm and a thickness of 1.5 mm with one, two, or three layers of AA1050 in the matrix of the AA5056 alloy (Figure 3, samples 1L, 2L, and 3L, respectively) were cut from the composite volume. HPT processing was conducted with varying numbers of revolutions n (ranging from 0.25 to 10) under a pressure of 6 GPa at room temperature. The photo of the sample after HPT treatment is shown in Figure S1a in the Supplementary Materials. The true accumulated strain, using the von Mises criterion at a distance of r = 5 mm from the center of the disk, was determined according to the following relation [24]:

$$\varepsilon_{vM} = \frac{1}{\sqrt{3}} \frac{2\pi r n}{h} \quad (1)$$

where h = 1 mm is the thickness of the sample.

Flat dog-bone-shaped specimens with a gauge part of 2 × 6 mm^2 were cut from the disks according to the schematic (Figure S1b of the Supplementary Materials). The sample surfaces were polished using SiC polishing papers starting with P400 and gradually decreasing down to P1500 while also changing the direction of polishing. Uniaxial tensile tests were performed on a Shimadzu AG-50kNX testing machine at a constant strain rate of 10^{-3} s^{-1}. At least three samples were tested for each state. The average values of the yield stress ($\sigma_{0.2}$), the ultimate tensile strength (σ_{UTS}), and the relative elongation to failure (δ) were determined from the obtained stress–strain diagrams.

The microstructure of the material was investigated by scanning electron microscopy (SEM) Mira Tescan 3 (Tescan, Brno, Czech Republic) at an accelerating voltage of 20 kV.

Chemical analysis of the samples was performed using an energy-dispersive X-ray (EDX) detector and the Oxford AZtec console (Oxford Instruments NanoAnalysis, Abingdon, Oxfordshire, UK). X-ray diffraction (XRD) analysis was performed on a Bruker D8 DISCOVER diffractometer (Billerica, MA, USA) in symmetric θ–2θ scan modes using a parallel beam of CuKα radiation (40 kV, 40 mA). The scanning step was 0.02°, and the time of exposure was 0.5 s. The average sizes of the coherent scattering domains (C) were determined via the full-profile Pauli simulation using the TOPAS 5.0 software.

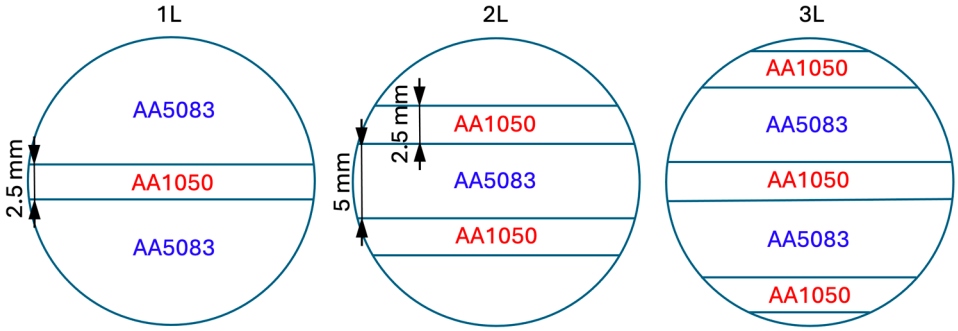

Figure 3. Configuration of samples for HPT processing obtained by WAAM.

3. Results and Discussion

3.1. Results of Tensile Tests

3.1.1. Composite Materials in Coarse-Grain State

The deformation behavior of the samples with an AA1050 layer aligned at 45° and 90° relative to the working part of the sample revealed several critical mechanical distinctions (Figure 4a). When the AA1050 layer was aligned at 90° or 45° to the loading axis, the composite demonstrated ultimate tensile strengths of 211 MPa and 216 MPa, respectively, which were approximately 20–25% lower than those of the original AA5056 alloy. This suggests that the incorporation of the AA1050 layer reduces the overall strength of the composite. However, it should be noted that the composite's strength remains significantly higher than that of the individual AA1050 component (data for AA1050_Wire in Table 1), indicating effective load sharing and support from the surrounding AA5056 matrix.

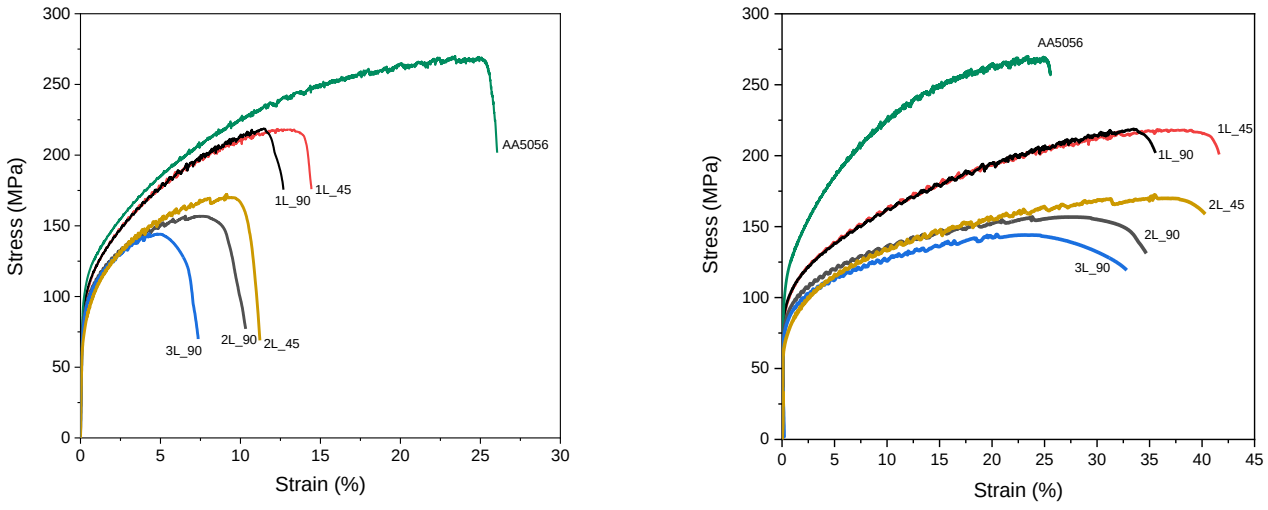

Figure 4. Stress–strain diagrams of composite materials: (**a**) measured based on the initial length of the working part, and (**b**) measured based on the localization of plastic deformation in the pure aluminum strip. Adapted from Ref. [31].

Table 1. Mechanical properties of different composite samples in comparison with initial raw materials. $\sigma_{0.2}$—yield stress; σ_{UTS}—ultimate tensile strength; δ_1—relative elongation to failure, based on the initial length of the working part; and δ_2—relative elongation to failure, based on the localization of plastic deformation in pure aluminum layers and in the transition zone of mixing.

	$\sigma_{0.2}$, MPa	σ_{UTS}, MPa	δ_1, %	δ_2, %
AA5056_Wire	159 ± 2	313 ± 1	31 ± 2	31 ± 2
AA1050_Wire	45 ± 1	78 ± 1	45 ± 4	45 ± 4
AA5056	111 ± 4	273 ± 4	26 ± 1	26 ± 1
1L_90	100 ± 1	211 ± 3	10 ± 1	35 ± 2
1L_45	98 ± 1	216 ± 3	13 ± 1	43 ± 2
2L_90	94 ± 1	155 ± 1	9 ± 0.5	34 ± 2
2L_45	77 ± 3	160 ± 5	10 ± 1	42 ± 2
3L_90	85 ± 4	140 ± 3	6 ± 0.5	33 ± 3

Figure 5 shows the tensile fracture surfaces of the tested specimens, illustrating that the crack followed the layer's inclination (45 and 90°) and the deformations were localized in the AA1050 layer (Figure 5c,f). The 1L_45 specimen exhibited a slightly higher tensile strength than the one with the band that was oriented at 90°. This difference in strength can be attributed to the increased volume of the AA1050 alloy in the working part of the sample, which helps to distribute the load more evenly, improving the mechanical performance and delaying fracture onset.

Increasing the number of AA1050 layers in the AA5056 matrix (2L_90 and 2L_45 samples) reduced the strength by about 20–25% compared to single-layer samples. Adding more AA1050 layers did not result in a proportionate decrease in strength. This can be explained by the competition for strain localization among the layers. In most specimens tested, one of the three AA1050 layers remained virtually undeformed, indicating that stress distribution becomes uneven within the composite as the number of layers increases. Certain layers take on a disproportionate share of the plastic deformation.

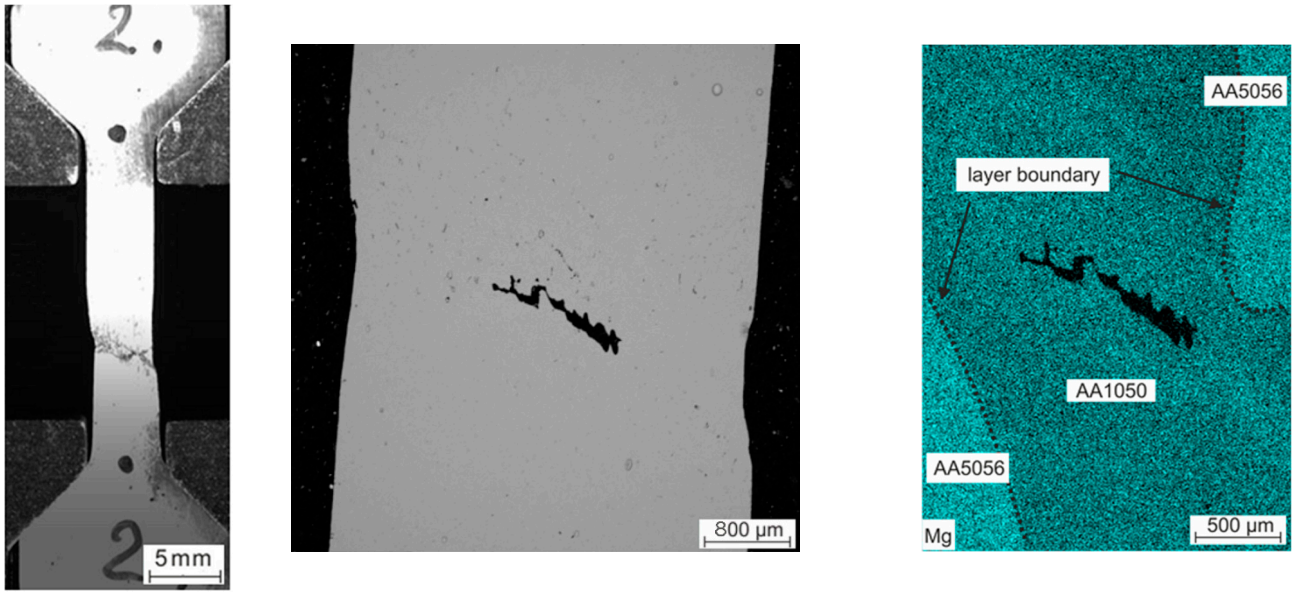

(**a**) (**b**) (**c**)

Figure 5. *Cont.*

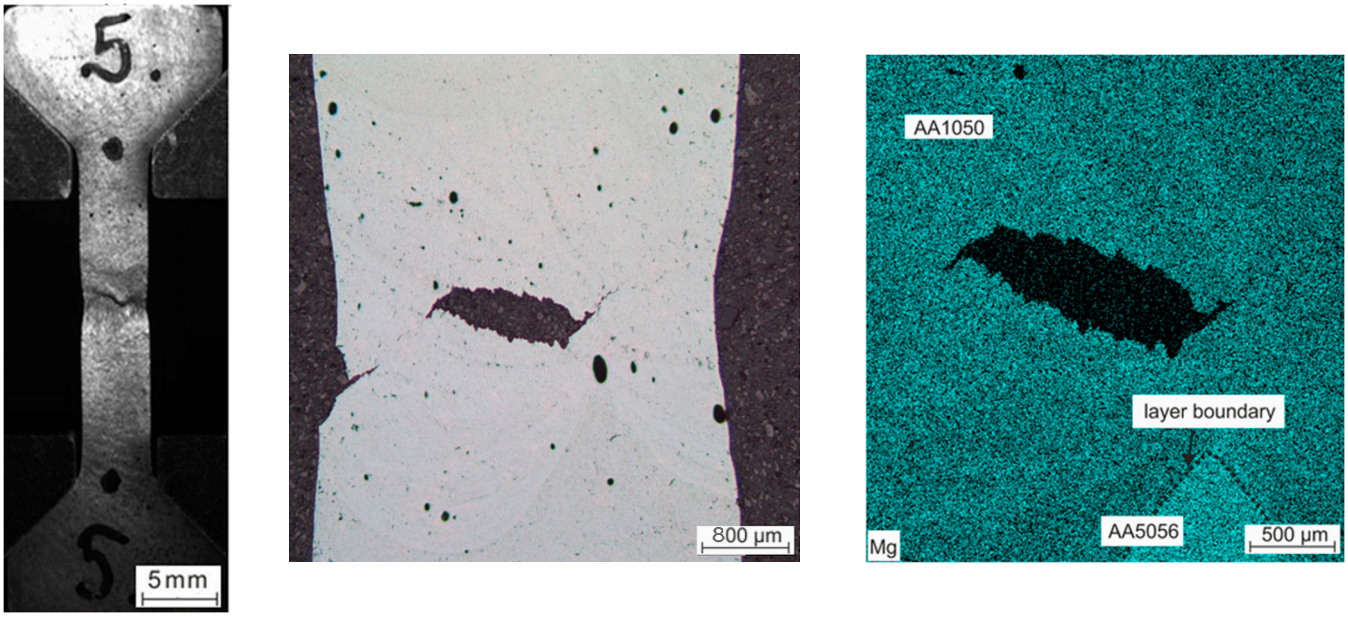

(**d**) (**e**) (**f**)

Figure 5. The view of the tensile testing process and the fracture surface of the central part of the 1L_45 sample (**a**–**c**) and the 1L_90 sample (**d**–**f**).

Table 1 provides the mechanical properties of the initial raw material used in the fabrication process (AA5056_Wire). The AA5056_Wire has the highest ultimate tensile strength ($\sigma_{UTS} \approx 313$ MPa) due to originally induced work hardening during its manufacture. The WAAM-processed AA5056 material shows a strength reduction of approximately 40 MPa compared to the initial wire. This decrease in strength is due to the melting and solidification processes that occur during the WAAM, which eliminate the work hardening introduced during wire drawing.

When analyzing the data presented in Figure 4a and Table 1, we observed a significant reduction in the plastic properties of the composite materials as the number of AA1050 layers within the AA5056 matrix increased. However, it is important to carefully interpret the deformation behavior. In Figure 4a, the percentage elongation was calculated using the standard formula for deformation:

$$\varepsilon = \frac{\Delta L}{L_0} \quad (2)$$

where ΔL represents the change in the specimen length during tensile testing, and L_0 is the initial specimen length.

It is important to note that the AA5056 specimens exhibited a uniform deformation across their entire length without any signs of localized deformation. In contrast, the composite materials showed a distinct localization in the AA1050 layer and in the transition zone of mixing, as shown in Figure 5. Due to this difference in deformation behavior, it is difficult to directly compare the elongation to failure values between the AA5056 and composite samples. Specifically, because of the localized nature of deformation in composites, the initial gauge lengths used for these materials are significantly different from those used for the uniform deformation of AA5056. According to the EDX analysis data (Figure 5b,e), for the 1L_45 and 1L_90 samples, the length of the deformable area is ~5 mm. For the 2L and 3L samples, we can assume that it is ~10 and ~15 mm, respectively. Based on this assumption, recalculated deformation diagrams were plotted in Figure 4b. The results, based on this assumption, show that the elongation to failure values in the composite samples approach those of the AA1050 wire (Table 1).

3.1.2. Composite Materials in Ultrafine-Grained State

Figure 6a shows the results of tensile testing for the composite material at different levels of strain (ε_{vM}). HPT processing resulted in a significant increase in strength after only 0.25 turns (corresponding to $\varepsilon_{vM} \approx 4.5$), but the material's ductility decreased (curve 2L_HPT_0.25). As the strain increased, both the 1L and 2L samples exhibited a general trend of increased strength and decreased ductility. For the 2L samples, the experiment was carried out over a wide range of ε_{vM} (Figure 6b). It is shown that increasing the strain to $\varepsilon_{vM} \approx 18$ (2L_HPT_1 sample) provided an optimal combination of ultimate tensile strength, yield stress, and ductility (Table 2). Further increases in strain led to a decrease in the plastic properties of the composite, likely due to the intense mixing of its components. At the highest strain level of $\varepsilon_{vM} \approx 181$, the material still retained some ductility and exhibited a σ_{UTS} of approximately 620 MPa. The best strength–ductility combination of the composite material (σ_{UTS} = 664 MPa, $\delta \approx 7\%$) was achieved for the 1L_HPT_2. The results of the mechanical testing for all samples are summarized in Table 2.

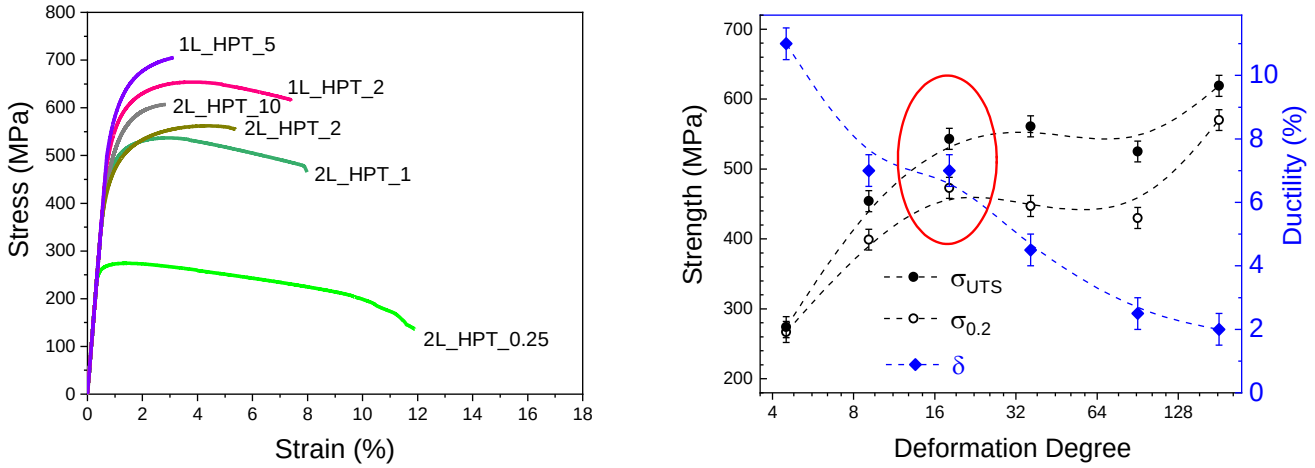

(**a**) (**b**)

Figure 6. Stress–strain diagrams for composite material samples with varying degrees of deformation (**a**), and dependences of the yield stress ($\sigma_{0.2}$), ultimate tensile strength (σ_{UTS}), and relative elongation to failure (δ) on the degree of deformation for the composite material with the initial configuration of 2L (**b**). The area of the optimal combination of properties is circled in red.

Table 2. Mechanical properties of composite material after HPT treatment. $\sigma_{0.2}$—yield stress; σ_{UTS}—ultimate tensile strength; δ—relative elongation to failure; and ε_{vM}—the true accumulated strain.

State	ε_{vM}	σ_{UTS} (MPa)	$\sigma_{0.2}$ (MPa)	δ (%)
1L_HPT_2	36	664 ± 10	570 ± 10	7 ± 1
1L_HPT_5	91	705 ± 11	587 ± 10	2 ± 0.5
1L_HPT_10	181	611 ± 15	590 ± 5	~0.5
2L_HPT_0.25	4.5	274 ± 10	267 ± 10	11 ± 1
2L_HPT_0.5	9	454 ± 15	399 ± 15	7 ± 2
2L_HPT_1	18	543 ± 5	473 ± 10	7 ± 1
2L_HPT_2	36	561 ± 5	447 ± 5	4.5 ± 0.5
2L_HPT_5	91	525 ± 15	430 ± 15	2.5 ± 0.5
2L_HPT_10	181	619 ± 15	570 ± 5	2 ± 0.5

It is well known that a similar HPT treatment (with $\varepsilon_{vM} \approx 181$) of commercially pure Al and Al–4.5Mg alloy leads to a grain structure refinement up to ~800 nm and ~200 nm, correspondingly [32,33]. As shown earlier, the conventional Al–4.5Mg alloy treated in a similar way demonstrates brittle behavior with a σ_{UTS} of 725 MPa [33]. On the other hand, the tensile strength of commercially pure aluminum treated in the same way was 185 MPa after HPT, with a uniform deformation of 2% [34]. In this study, we created a material that combined the strength of nanostructured industrial alloyswith the plasticity of nanocrystalline commercially pure aluminum. This effect was achieved due to the presence of the AA1050 layer within the AA5056 matrix, which locally enhanced the plastic deformation characteristics of the composite. Despite the overall decrease in strength due to the softer AA1050 phase, this layer plays an important role in improving localized ductility.

3.2. Characterisation of the Microstructure of Composite Materials

The AA1050 alloy is a pure aluminum alloy, and in this study, we focused on the magnesium content in both the AA5056 and AA1050 layers to evaluate their mixing. The presence of magnesium in the AA1050 layer indicates effective mixing between the layers, while its absence suggests minimal or no mixing. Figure 7a presents a map of magnesium distribution for a sample with one layer of AA1050. Figure 7b shows the magnesium content along line 1, marked in Figure 7a. These data clearly show that during the production of layered materials through direct energy deposition, the layers undergo significant mixing. Specifically, the magnesium content in the AA5056 layer was approximately 5 wt.%, while the Mg content in the AA1050 layer reached about 2.5 wt.% with a transition zone spanning approximately 250 µm. These findings explain why the strength of the layered composite exceeds that of its weaker constituent.

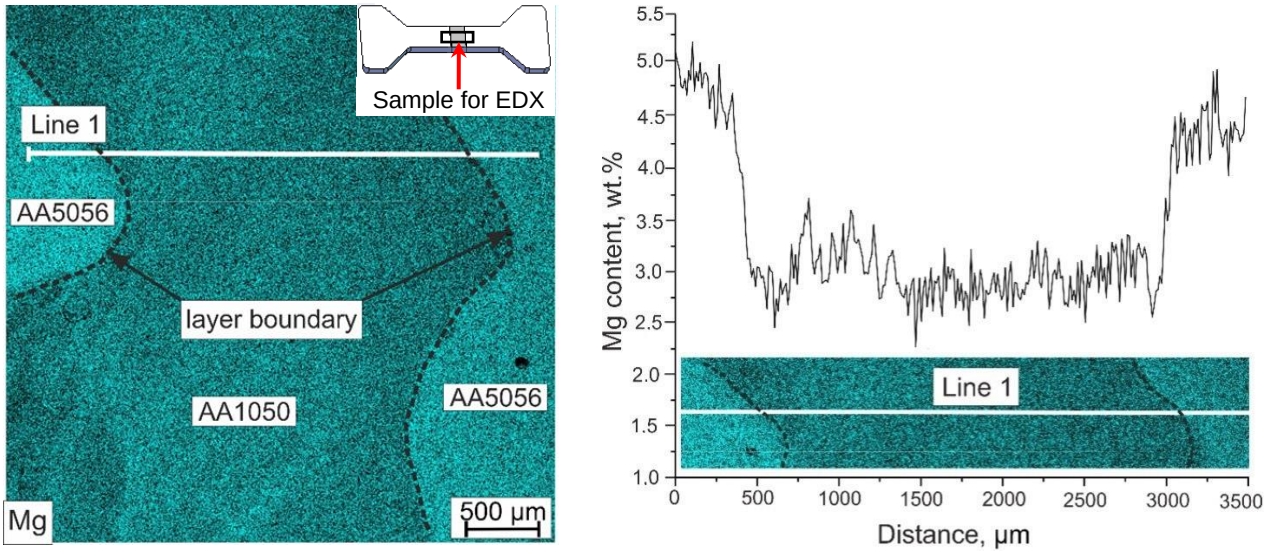

(**a**) (**b**)

Figure 7. EDX results: Mg distribution (**a**) and the location of the EDX specimen (the inset) and results of Mg content determination on line 1 (**b**).

Figure 8 shows the Mg distribution in the 2L_HPT_1 sample (Figure 8a) and the chemical profile of the Mg content along lines 1 and 2 (Figure 8b). As can be seen, the sample contains areas with an increased concentration of magnesium corresponding to the concentration of Mg in the initial alloy AA5056, as well as areas with a content of Mg ~2 wt.%. This indicates that materials are being mixed during the HPT process, and the distribution of magnesium in the sample volume is changing.

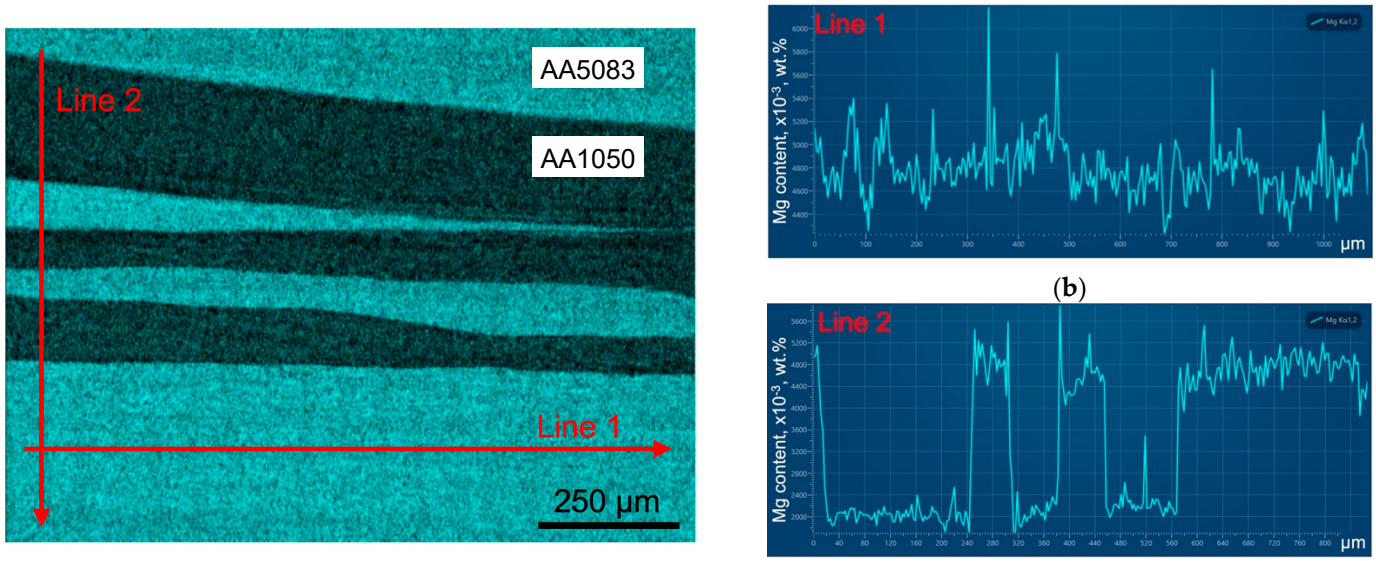

(**a**) (**b**) (**c**)

Figure 8. Mg distribution in the 2L_HPT_1 composite sample (**a**), the chemical profile of the Mg content along lines 1 (**b**) and 2 (**c**).

The obtained X-ray diffraction pattern of the 1L_HPT_2 sample is shown in Figure 9. There are no secondary phases revealed, but the results of the modeling confirm that the material consists of two substructures. The determined values of the coherent scattering domains are ~250 nm and >1000 nm for the first and the second substructures, correspondingly. The phase volume ratio is approximately 80/20, which corresponds to the volume ratio of materials in the initial 1L sample.

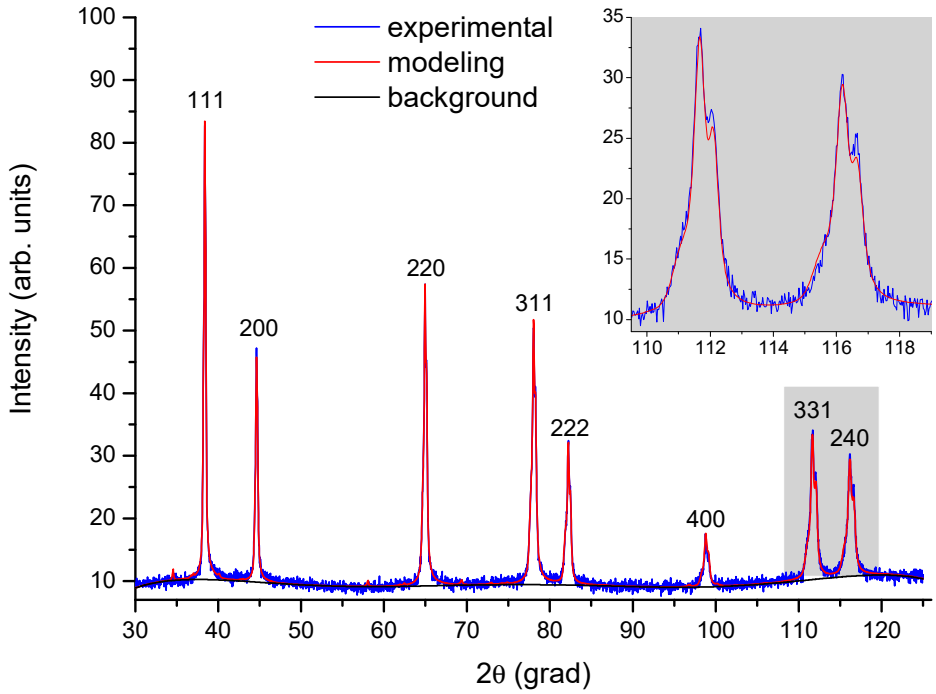

Figure 9. XRD pattern of the 1L_HPT_2 composite sample.

4. Conclusions

The results of this study demonstrate the potential of wire arc additive manufacturing for producing layered aluminum composites. Specifically, we focused on composites composed of AA1050 and AA5056 alloys, with AA1050 incorporated as a 2.5 mm thick layer into the robust AA5056 matrix. We investigated the deformation characteristics of these composites and found that, despite the significant difference in tensile strength between the two alloys, the overall strength of the composite remained relatively stable. The addition of the lower-strength AA1050 alloy enhanced localized plasticity in the composite, which can be beneficial for parts with complex geometries. This localized plasticity contributes to the safety of structural components manufactured using additive technologies. Our study also focused on the influence of accumulated strain induced by high-pressure torsion treatment on the mechanical properties and microstructure of a composite material. We analyzed the relationships between static strength, plasticity, and microstructural evolution, leading to the identification of an optimal deformation path for achieving a favorable balance of mechanical properties.

The main conclusions from this work can be summarized as follows:

1. The combination of WAAM technology and HPT allows precise control over the volume ratio of constituent materials in composite samples.
2. Optimal strength and ductility are achieved in composite samples containing one or two layers of commercially pure aluminum subjected to deformation levels of approximately 36% and 18%, respectively.
3. The observed combination of high strength and plasticity can be attributed to the bimodal microstructure, as confirmed by microstructural analysis.

Supplementary Materials: The following supporting information can be downloaded at: https://www.mdpi.com/article/10.3390/met14121445/s1, Figure S1: Photo of sample after HPT treatment (a); schematic of cutting-out of tensile test samples (b).

Author Contributions: Conceptualization, A.E.; methodology, A.E.; validation, A.E. and A.M.; investigation, A.E., A.M. and D.V.; resources, A.V.; writing—original draft preparation, A.E., A.M., A.V. and D.V.; writing—review and editing, A.M.; visualization, A.E. and A.M.; supervision, A.E.; and project administration, A.E. All authors have read and agreed to the published version of the manuscript.

Funding: Deformation-heat treatment and studies of microstructure and mechanical properties were funded by the Russian Science Foundation, grant number 22-79-10043. The production of the composite material by WAAM technology was funded by the World-class Research Center program: Advanced Digital Technologies (Contract no. 075-15-2022-312 dated 20 April 2022).

Data Availability Statement: The raw data supporting the conclusions of this article will be made available by the authors on request.

Acknowledgments: The mechanical and structural studies were performed using the equipment from the "Centre for the Study of Extreme States of Materials and Constructions", the "Cryogenic department", and the "Centre for X-ray Diffraction Studies" at the Research Park of St. Petersburg State University.

Conflicts of Interest: The authors declare no conflicts of interest.

References

1. Mondolfo, L.F. *Aluminum Alloys: Structure and Properties*; Elsevier: Amsterdam, The Netherlands, 1976. [CrossRef]
2. Aluminum Association. *Aluminum: Properties and Physical Metallurgy*; ASM International: Detroit, MI, USA, 1984.
3. Ding, D.; Pan, Z.; Cuiuri, D.; Li, H. Wire-feed additive manufacturing of metal components: Technologies, developments and future interests. *Int. J. Adv. Manuf. Technol.* **2015**, *81*, 465–481. [CrossRef]
4. Williams, S.W.; Martina, F.; Addison, A.C.; Ding, J.; Pardal, G.; Colegrove, P. Wire+ arc additive manufacturing. *Mater. Sci. Technol.* **2016**, *32*, 641–647. [CrossRef]
5. Gress, D.R.; Kalafsky, R.V. Geographies of production in 3D: Theoretical and research implications stemming from additive manufacturing. *Geoforum* **2015**, *60*, 43–52. [CrossRef]

6. Evans, S.I.; Wang, J.; Qin, J.; He, Y.; Shepherd, P.; Ding, J. A review of WAAM for steel construction–Manufacturing, material and geometric properties, design, and future directions. *Structures* **2022**, *44*, 1506–1522. [CrossRef]
7. Munusamy, S.; Jerald, J. Effect of build orientation on the microstructure and mechanical properties of wire arc additive manufactured grade 91 steel/monel 400 bimetallic components. *Vacuum* **2024**, *227*, 113429. [CrossRef]
8. Kesarwani, S.; Yuvaraj, N.; Niranjan, M.S. Impact of depositional direction and current on microstructure and mechanical properties of the bimetallic wall of ER5356/ER4043 fabricated by cold metal transfer based wire arc additive manufacturing. *CIRP J. Manuf. Sci. Technol.* **2024**, *53*, 17–33. [CrossRef]
9. Ayan, Y.; Kahraman, N. Fabrication and characterization of functionally graded material (FGM) structure containing two dissimilar steels (ER70S-6 and 308LSi) by wire arc additive manufacturing (WAAM). *Mater. Today Commun.* **2022**, *33*, 104457. [CrossRef]
10. Jadhav, S.; Bajestani, M.S.; Islam, S.; Karim, M.A.; Kim, C.J.; Lee, H.-J.; Cho, Y.T.; Kim, D.B. Materials characterization of Ti6Al4V to NbZr1 bimetallic structure fabricated by wire arc additive manufacturing. *Mater. Today Commun.* **2023**, *36*, 106934. [CrossRef]
11. Karim, M.A.; Jadhav, S.; Kannan, R.; Pierce, D.; Lee, Y.; Nandwana, P.; Kim, D.B. Investigating stainless steel/aluminum bimetallic structures fabricated by cold metal transfer (CMT)-based wire-arc directed energy deposition. *Addit. Manuf.* **2024**, *81*, 104015. [CrossRef]
12. Spalek, N.; Brunow, J.; Braun, M.; Rutner, M. WAAM-Fabricated Laminated Metal Composites. *Metals* **2021**, *11*, 1948. [CrossRef]
13. Singh, S.R.; Khanna, P. Wire arc additive manufacturing (WAAM): A new process to shape engineering materi-als. *Mater. Today Proc.* **2020**, *44*, 118–128. [CrossRef]
14. Yu, L.; Chen, K.; Zhang, Y.; Liu, J.; Yang, L.; Shi, Y. Microstructures and mechanical properties of NiTi shape memory alloys fabricated by wire arc additive manufacturing. *J. Alloys Compd.* **2022**, *892*, 162193. [CrossRef]
15. Chaturvedi, M.; Scutelnicu, E.; Rusu, C.; Mistodie, L.; Mihailescu, D.; Subbiah, A. Wire Arc Additive Man-ufacturing: Review on Recent Findings and Challenges in Industrial Applications and Materials Characterization. *Metals* **2021**, *11*, 939. [CrossRef]
16. Panchenko, O.; Kurushkin, D.; Mushnikov, I.; Khismatullin, A.; Popovich, A. A high-performance WAAM process for Al–Mg–Mn using controlled short-circuiting metal transfer at increased wire feed rate and increased travel speed. *Mater. Des.* **2020**, *195*, 109040. [CrossRef]
17. Salomatova, E.S.; Kartashev, M.F.; Trushnikov, D.N.; Permykov, G.L.; Olshanskaya, T.V.; Abashev, I.R.; Fedoseeva, E.M.; Koleva, E.G. Evaporation processes of alloying components during wire-arc deposition of aluminum alloy 5056. *IOP Conf. Ser. Mater. Sci. Eng.* **2020**, *758*, 012064. [CrossRef]
18. Mavlyutov, A.; Evstifeev, A.; Volosevich, D.; Gushchina, M.; Voropaev, A.; Zotov, O.; Klimova-Korsmik, O. The Effect of Severe Plastic Deformation on the Microstructure and Mechanical Properties of Composite from 5056 and 1580 Aluminum Alloys Produced with Wire Arc Additive Manufacturing. *Metals* **2023**, *13*, 1281. [CrossRef]
19. Gu, J.; Wang, X.; Bai, J.; Ding, J.; Williams, S.; Zhai, Y.; Liu, K. Deformation microstructures and strengthening mechanisms for the wire-arc additively manufactured Al-Mg4.5Mn alloy with inter-layer rolling. *Mater. Sci. Eng. A* **2018**, *712*, 292–301. [CrossRef]
20. Li, S.; Zhang, L.J.; Ning, J.; Wang, X.; Zhang, G.F.; Zhang, J.X.; Na, S.J.; Fatemeh, B. Comparative study on the microstructures and properties of wire-arc additively manufactured 5356 aluminum alloy with argon and nitrogen as the shielding gas. *Addit. Manuf.* **2020**, *34*, 101206. [CrossRef]
21. Sabirov, I.; Murashkin, M.Y.; Valiev, R.Z. Nanostructured aluminium alloys produced by severe plastic deformation: New horizons in development. *Mater. Sci. Eng. A* **2013**, *560*, 1–24. [CrossRef]
22. Zhilyaev, A.P.; Langdon, T.G. Using high-pressure torsion for metal processing: Fundamentals and applications. *Prog. Mater. Sci.* **2008**, *53*, 893–979. [CrossRef]
23. Edalati, K.; Horita, Z. A review on high-pressure torsion (HPT) from 1935 to 1988. *Mater. Sci. Eng. A* **2016**, *652*, 325–352. [CrossRef]
24. Valiev, R.; Islamgaliev, R.; Alexandrov, I. Bulk nanostructured materials from severe plastic deformation. *Prog. Mater. Sci.* **2000**, *45*, 103–189. [CrossRef]
25. Kalsar, R.; Yadav, D.; Sharma, A.; Brokmeier, H.G.; May, J.; Höppel, H.W.; Skrotzki, W.; Suwas, S. Effect of Mg content on microstructure, texture and strength of severely equal channel angular pressed aluminium-magnesium alloys. *Mater. Sci. Eng. A* **2020**, *797*, 140088. [CrossRef]
26. Liu, M.P.; Roven, H.J.; Murashkin, M.Y.; Valiev, R.Z.; Kilmametov, A.; Zhang, Z.; Yu, Y. Structure and mechanical properties of nanostructured Al-Mg alloys processed by severe plastic deformation. *J. Mater. Sci.* **2013**, *48*, 4681–4688. [CrossRef]
27. Liu, Y.; Liu, M.; Chen, X.; Cao, Y.; Roven, H.J.; Murashkin, M.; Zhou, H. Effect of Mg on microstructure and mechanical properties of Al-Mg alloys produced by high pressure torsion. *Scr. Mater.* **2019**, *159*, 137–141. [CrossRef]
28. Murashkin, M.Y.; Kil'Mametov, A.R.; Valiev, R.Z. Structure and mechanical properties of an aluminum alloy 1570 subjected to severe plastic deformation by high-pressure torsion. *Phys. Met. Metall.* **2008**, *106*, 90–96. [CrossRef]
29. Liu, M.; Zheng, R.; Ma, C.; Tsuji, N. Ultra-strong, ductile and thermally stable ultrafine grained 5083 Al alloy fabricated by high pressure torsion using pre-sintered powders. *Materialia* **2019**, *8*, 100448. [CrossRef]
30. Chen, Y.; Liu, M.; Ding, L.; Jia, Z.; Jia, S.; Wang, J.; Murashkin, M.; Valiev, R.Z.; Roven, H.J. Atomic-scale inhomogeneous solute distribution in an ultrahigh strength nanocrystalline Al-8 Mg aluminum alloy. *Mater. Charact.* **2023**, *198*, 112706. [CrossRef]
31. Evstifeev, A.D.; Yakupov, B.A.; Mavlyutov, A.M.; Volosevich, D.V.; Voropaev, A.A. Mechanical properties of layered composites based on AA1050 and AA5056 aluminum alloys produced by WAAM technology. *J. Phys. Conf. Ser.* **2024**, *2817*, 012012. [CrossRef]

32. Orlova, T.; Mavlyutov, A.; Bondarenko, A.; Kasatkin, I.; Murashkin, M.; Valiev, R. Influence of grain boundary state on electrical resistivity of ultrafine grained aluminium. *Philos. Mag.* **2016**, *96*, 2429–2444. [CrossRef]
33. Evstifeev, A.; Smirnov, I. Effect of annealing and additional deformation on the microstructure and mechanical properties of ultrafine-grained Al5083 alloy. *Mater. Phys. Mech.* **2023**, *95*, 20–28. [CrossRef]
34. Mavlyutov, A.M.; Latynina, T.A.; Murashkin, M.Y.; Valiev, R.Z.; Orlova, T.S. Effect of annealing on the microstructure and mechanical properties of ultrafine-grained commercially pure Al. *Phys. Solid State* **2017**, *59*, 1970–1977. [CrossRef]